ADVANCED FUNCTIONAL MATERIALS
www.afm-journal.de

Copper Thiophosphate (Cu_3PS_4) as Electrode for Sodium-Ion Batteries with Ether Electrolyte

*Wolfgang Brehm, Aggunda L. Santhosha, Zhenggang Zhang, Christof Neumann, Andrey Turchanin, Andréa Martin, Nicola Pinna, Martin Seyring, Markus Rettenmayr, Johannes R. Buchheim, and Philipp Adelhelm**

Lithium and sodium thiophosphates (and related compounds) have recently attracted attention because of their potential use as solid electrolytes in solid-state batteries. These compounds, however, exhibit only limited stability in practice as they react with the electrodes. The decomposition products partially remain redox active hence leading to excess capacity. The redox activity of thiophosphates is explicitly used to act as electrode for sodium-ion batteries. Copper thiophosphate (Cu_3PS_4) is used as a model system. The storage behavior between 0.01 and 2.5 V versus Na^+/Na is studied in half cells using different electrolytes with 1 M $NaPF_6$ in diglyme showing the best result. Cu_3PS_4 shows highly reversible charge storage with capacities of about 580 mAh g^{-1} for more than 200 cycles @120 mA g^{-1} and about 450 mAh g^{-1} for 1400 cycles @1 A g^{-1}. The redox behavior is studied by operando X-ray diffraction and X-ray photoelectron spectroscopy. During initial sodiation, Cu_3PS_4 undergoes a conversion reaction including the formation of Cu and Na_2S. During cycling, the redox activity seems dominated by sulfur. Interestingly, the capacity of Cu_3PS_4 for lithium storage is smaller, leading to about 170 mAh g^{-1} after 200 cycles. The results demonstrate that thiophosphates can lead to reversible charge storage over several hundred cycles without any notable capacity decay.

1. Introduction

Sodium-ion batteries (NIBs) are currently developed with the aim to provide an alternative to lead–acid and lithium-ion batteries that is based on more abundant and low-cost materials. The progress in the field is frequently summarized in literature.[1,2] For the positive electrodes, the field is especially profiting from the rich chemistry of layered oxides, polyanion compounds and Prussian blue analogues, which allows tuning of the electrode properties.[3] To reduce cost, compounds rich in abundant Mn and Fe are preferred over Co and Ni that dominate the cathode materials for most lithium-ion batteries (LIBs). The composition of the electrolyte solutions is largely adopted from LIBs with carbonates as solvents and $NaPF_6$ as conductive salt though also ethers are increasingly being studied as well as polymer and inorganic solid electrolytes.[4] Considering potential negative electrodes, however, the materials choice is presently rather limited. Graphite, being the standard material in lithium-ion batteries, can only be applied using solvent cointercalation phenomena in ether electrolytes.[5] The capacity, however, is limited to around 110 mAh g^{-1} so far and the electrode undergoes large volume changes during cycling.[6] Higher capacities can be achieved in disordered carbons,[7] but much of the capacity is obtained at potentials likely too close to the sodium metal plating potential to enable safe operation. Various titanium oxides and related compounds are of interest too because titanium is quite abundant. The capacities, however, are often well below 200 mAh g^{-1}.[8] From the class of metals and metalloids, only Sn, Sb, and Pb show high storage capacities.[1e,9] While the volume expansion on the electrode level can be

W. Brehm, A. L. Santhosha, Z. Zhang, Dr. J. R. Buchheim, Prof. P. Adelhelm
Institute of Technical Chemistry and Environmental Chemistry
Friedrich Schiller University Jena
Philosophenweg 7a, Jena 07743, Germany
E-mail: philipp.adelhelm@hu-berlin.de

The ORCID identification number(s) for the author(s) of this article can be found under https://doi.org/10.1002/adfm.201910583.

© 2020 The Authors. Published by WILEY-VCH Verlag GmbH & Co. KGaA, Weinheim. This is an open access article under the terms of the Creative Commons Attribution License, which permits use, distribution and reproduction in any medium, provided the original work is properly cited.

DOI: 10.1002/adfm.201910583

A. L. Santhosha, Z. Zhang, A. Martin, Prof. N. Pinna, Prof. P. Adelhelm
Institut für Chemie
Humboldt-Universität zu Berlin
Brook-Taylor-Str. 2, Berlin 12489, Germany

C. Neumann, Prof. A. Turchanin
Institute of Physical Chemistry
Friedrich Schiller University Jena
Lessingstraße 10, Jena 07743, Germany

Prof. A. Turchanin, Prof. M. Rettenmayr, Prof. P. Adelhelm
Center for Energy and Environmental Chemistry Jena (CEEC Jena)
Philosophenweg 7a, Jena 07743, Germany

M. Seyring, Prof. M. Rettenmayr
Otto-Schott-Institute of Materials Research
Friedrich Schiller University Jena
Löbdergraben 32, Jena 07743, Germany

effectively buffered by embedding the particles in a carbon matrix, the widespread use might be limited as these elements are not abundant. Moreover, Pb, Sb and their compounds are not environmentally friendly and/or toxic. For high capacity electrodes, this largely leaves conversion electrodes as options.[10] These are based on transition metal compounds, often oxides or sulfides. During sodiation/lithiation, the transition metal is fully reduced along with formation of sodium/lithium oxides or sulfides. Depending on the transition metal and the type of anion (oxides, sulfides, fluorides, ...) used, the properties of these electrodes can strongly vary. Common advantages are very high capacities easily reaching several hundred mAh g^{-1}, while common challenges are sluggish kinetics leading to large voltage hysteresis, volume expansion, and low initial coulombic efficiency (ICE). Moreover, the reaction mechanisms are often nonideal, include amorphous and intermediate phases along with side reactions, see, e.g., results on CuO.[10a,11]

Recently, copper phosphides were investigated because of their very high theoretical volumetric or gravimetric capacities.[12] For example, Zhao et al. reported that CuP_2 has a theoretical capacity of q_{th} = 1282 mAh g^{-1}. In Na half cells, the practical storage capacity at 150 mA g^{-1} was about 450 mAh g^{-1} between the 2nd and 30th cycle (≈100% capacity retention). However, strong capacity fading occurred during prolonged cycling leaving only 170 mAh g^{-1} after 100 cycles.[12b] Cu_3P shows only a moderate theoretical capacity of 363 mAh g^{-1}, i.e., on par with graphite in lithium-ion batteries, but its volumetric capacity is approximately three times higher (2664 Ah l^{-1} vs 781 Ah l^{-1}). Stan et al. found stable cycling with 220 mAh g^{-1} after 50 cycles.[13]

Copper sulfides (CuS with q_{th} = 560 mAh g^{-1} and Cu_2S q_{th} = 337 mAh g^{-1}) are also well known as high capacity storage materials for LIBs and NIBs. Their high intrinsic electronic and ionic conductivity is a great advantage, but cycle life is poor in commonly used carbonate electrolytes.[14] Han et al. for example showed for a carbonate electrolyte a comparably high specific capacity of 582 mAh g^{-1} in the initial cycle, but only 13.8% after the first 10 cycles were retained for a Li half-cell.[15] Moreover, in another study from Debart et al. a similar high capacity value was achieved in the initial cycle, and they observed a drop to about 50 mAh g^{-1} after five cycles, explained by the dissolution of active material in the carbonate electrolyte.[16] Jache et al. could link this strong capacity fade to the electrolyte solvent and showed that the use of carbonates leads to short cycle life while ethers provide long cycle life. Bulk CuS and Cu_2S were used for this study, the latter showing the best cycle life.[14b] Using also an ether electrolyte, Wang et al. showed for nanostructured CuS that high capacities between 376 and 447 mAh g^{-1} are obtained for more than 100 cycles at C-rates up to 2C.[17] In case of sodium, Park et al. showed that the theoretical capacity of CuS can be almost reached after a longer activation period of around 100 cycles (0.2C).[18]

The combined use of copper, sulfur and phosphorous leads to the class of copper thiophosphates. Cu (6 \$ kg^{-1})[19] and especially P (0.45 \$ kg^{-1})[20] and S (0.1 \$ kg^{-1})[21] are cost-effective and abundant elements, making them attractive for application. It is interesting to note that lithium/sodium thiophosphates such as Li_3PS_4 and Na_3PS_4 are currently highly studied as solid electrolytes (SE) for all solid state batteries thanks to their high room temperature ionic conductivity in the order of ≈10^{-4}–10^{-2} S cm^{-1} and their high ductility.[22] Recent results, however, showed that the solid electrolytes easily decompose in contact with positive and negative electrodes as the theoretical electrochemical stability window is quite narrow.[23] Long-term use of these materials in high voltage batteries therefore requires the formation of suitable interphases that stabilize the electrode–electrolyte contact areas.[22b,e,23b] In analogy to conventional lithium-ion batteries, formation of a solid electrolyte interphase (SEI) is desired, yet this is not a trivial task. Decomposition products of the solid electrolyte, however, can also remain redox active during cycling, hence leading to excess capacity. While this is not necessarily a problem, it can lead to a continuous cell degradation and an overestimation of the storage capacity of the electrode material.[23b] Calculations predicted that the electrochemical stability window for thiophosphate electrolytes is limited by sulfur and by phosphorus redox activity (depending on the redox potential).[23b,24]

Here, we intentionally use a thiophosphate not as solid electrolyte, but instead as electrode material Cu_3PS_4 is taken as a study case. To the best of our knowledge, the intentional use of thiophosphates as electrode material for NIBs has not been reported yet. Nevertheless, it is important to mention a very recent study by Fan et al., who reported on iron thiophosphite ($FePS_3$) and related compound.[25] According to their results, a composite electrode with reduced graphene oxide was synthesized and showed an initial capacity of about 880 mAh g^{-1} (0.05 A g^{-1}) in a Na half cell, however the ICE was only 48%. After the first cycle the capacity was around 420 mAh g^{-1}. Cycling led to a capacity fade of 58% over 300 cycles leading to 243 mAh g^{-1}. Higher capacities and better cycle life were achieved for lithium with 843 mAh g^{-1} found after 120 cycles. The ICE value was only 59%, however. Similar findings were observed in a study by Edison et al. about tin thiophosphite $SnPS_3$ in a Li half cell.[26] They obtained capacity values >2300 mAh g^{-1} in the initial cycle, but the ICE was even only 38%. However, still a capacity of 532 mAh g^{-1} after 100 cycles (0.1 A g^{-1}) was retained. Although improvement is necessary, these findings are a clear motivation to study the behavior of thiophosphates as electrodes in batteries. An advantage of Cu_3PS_4 over $FePS_3$ and $SnPS_3$ is the possibility to synthesize the former by simple reactive ball milling, while for the latter two more complex synthesis routes were applied. The Cu_3PS_4 was first prepared in a ball mill and then subsequently mixed with carbon black in a second ball milling step to prepare a Cu_3PS_4/C composite. Electrodes of the active material were tested for their sodium storage behavior in half cells. A variety of analytical tools (scanning and transmission electron microscopy (SEM, TEM), X-ray photoelectron spectroscopy (XPS) as well as operando X-ray diffraction (XRD) are applied to study the reaction mechanism. Electrochemical results are compared with the analogue lithium half cells.

2. Results and Discussion

2.1. Materials Characterization

Cu_3PS_4 was synthesized in a planetary ball mill (PBM) for 24 h at 400 rpm from stoichiometric amounts of Cu, sulfur and P_2S_5 according to

$$6Cu + P_2S_5 + 3S \rightarrow 2Cu_3PS_4 \quad (1)$$

© 2020 The Authors. Published by WILEY-VCH Verlag GmbH & Co. KGaA, Weinheim

The reaction product was confirmed by XRD, as shown in **Figure 1**. Cu_3PS_4 crystallizes in an orthorhombic structure and the pattern is well in line with the reference (ICSD: 98-041-2240). Rietveld refinement revealed lattice parameters of a = 7.254(5) Å, b = 6.305(5) Å, c = 6.041(2) Å (*Pmn*21 space group) and a crystallite size of 21 nm, see Figure S1 in the Supporting Information.

Local analysis was done using TEM combined with selected area electron diffraction (SAED), presented in **Figure 2**. The images show that the as-prepared Cu_3PS_4 consisted of polycrystalline agglomerates with high phase purity. SAED pattern and bulk powder XRD pattern are compared in Figure S2 (Supporting Information), showing good agreement. High resolution TEM images in Figure 2c show an interplanar lattice spacing of 3.09 Å (red) corresponding to the (002) planes, i.e., half of the length of the c-axis of the Cu_3PS_4 unit cell. Moreover, 6.39 Å were measured for the interplanar distance of the (100) lattice plane, which is in good agreement with the length of the b-axis of the Cu_3PS_4 unit cell. These results are well in line with the results of the Rietveld refinement of the XRD analysis in Figure 1. Overall, the results confirm that phase pure Cu_3PS_4 was obtained by the ball milling process. An important difference

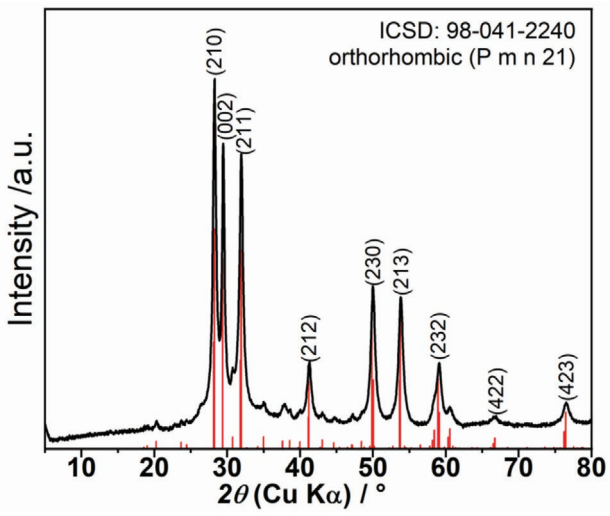

Figure 1. X-ray diffraction pattern of Cu_3PS_4 powder synthesized by high energy ball milling for 24 h in a planetary ball mill (ICSD: 98-041-2240). The obtained pattern corresponds to an orthorhombic crystal lattice of the *Pmn*21 space group.

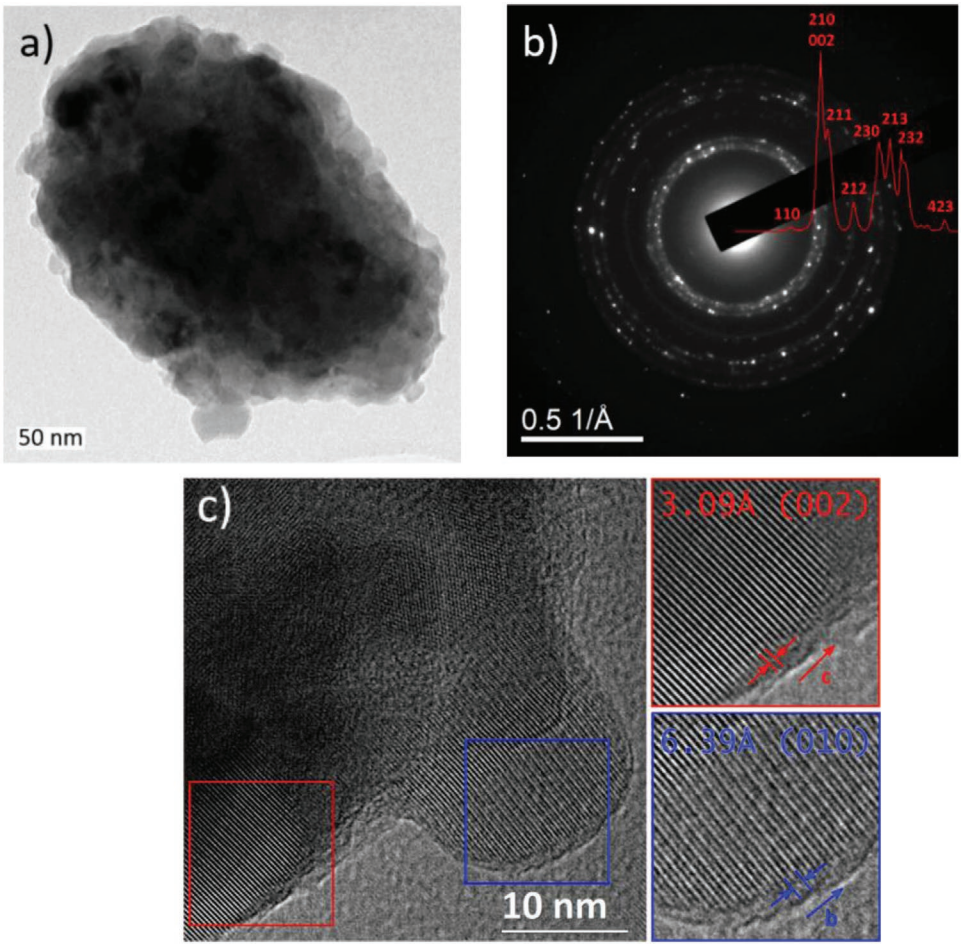

Figure 2. TEM analysis of the Cu_3PS_4 powder: a) single particle image; b) TEM/SAED pattern; c) HRTEM images of agglomerated Cu_3PS_4 crystals.

© 2020 The Authors. Published by WILEY-VCH Verlag GmbH & Co. KGaA, Weinheim

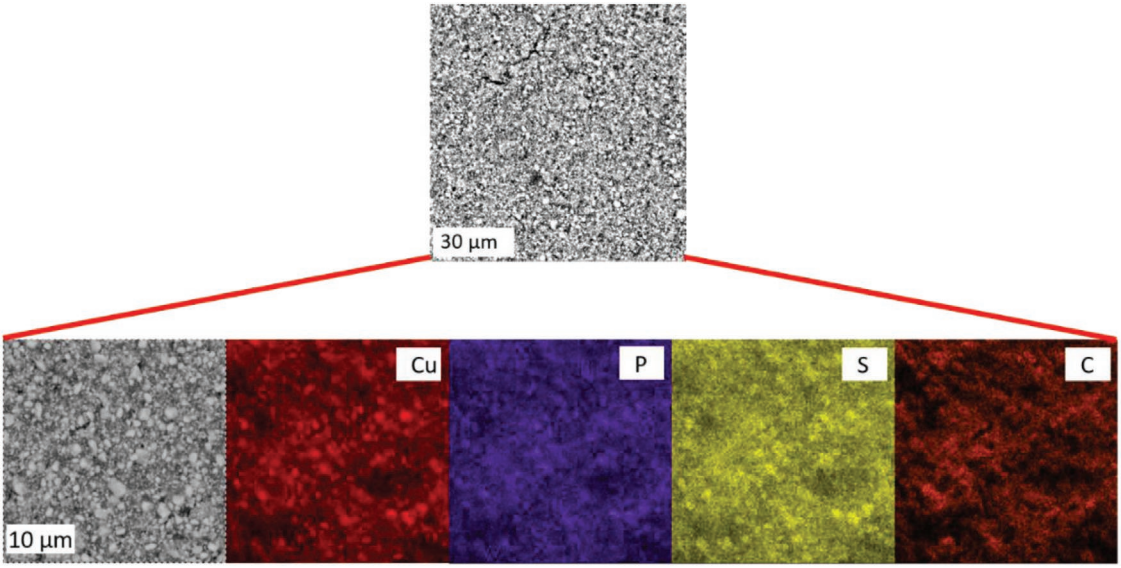

Figure 3. SEM images of the Cu_3PS_4/C composite electrode and EDS elemental mapping.

between Cu_3PS_4 and the thiophosphates Li_3PS_4 and Na_3PS_4 used for solid state batteries is that Cu_3PS_4 is air stable, while the latter compounds are highly hygroscopic, leading to immediate formation of H_2S upon air exposure. Cu_3PS_4 is also stable in ethanol as it was used in photo-electrochemical studies.[12e,27]

The synthesized Cu_3PS_4 was mixed with carbon black as conductive additive (7:3 by weight) in a swing ball mill (SBM) for 12 h (25 Hz) to form a Cu_3PS_4/C composite. Electrodes were then prepared by casting a slurry onto a copper current collector using PVDF as binder. The total composition of the electrode in weight fractions was Cu_3PS_4:C:PVDF = 0.66:0.29:0.05. SEM/EDS images of the electrodes shown in **Figure 3** reveal fine particles up to a few µm in size and a homogenous distribution of all elements suggesting that Cu_3PS_4 was intimately mixed with carbon. This observation is in line with the XRD results. A more detailed view on the particle size and the materials morphology can be seen in the TEM images shown in Figure S3a,b (Supporting Information). The particles presented in Figure S3a (Supporting Information) were captured directly after synthesis in the PBM. The synthesis leads to particles in different sizes ranging from around <100 nm up to about 1 µm. The embedment in the surrounding carbon matrix after the additional ball milling step with carbon can be seen in Figure S3b–d (Supporting Information). Herein, also larger aggregates >1 µm were observed. The particles show an irregular shape as expected, which can be seen with a more detailed view on Figure S3c,d (Supporting Information).

Thickness and loading of the electrodes were around 20 µm (without current collector) and between 1.5–2.2 mg cm^{-2}. Assuming an ideal and full conversion according to

$$Cu_3PS_4 + 11Na \rightleftarrows 3Cu + 4Na_2S + Na_3P \,|\, 843 \ \text{mAh g}^{-1} \quad (2)$$

would correspond to a theoretical areal capacity between 2.5–3.7 mAh cm^{-2}. All experiments presented in this manuscript were performed at a current density of 120 mA g^{-1}, using a solution of $NaPF_6$ (1 M) in diglyme as electrolyte.

2.2. Electrochemical Characterization of Cu_3PS_4

Voltage profiles are shown in **Figure 4**a,b. The initial cycle shows a discharge capacity of more than 1030 mAh g^{-1} (1.49 mAh cm^{-2}), followed by a charge capacity of 817 mAh g^{-1}. Sloping voltages and a large hysteresis are observed, which are typical for conversion reactions. However, some distinct features can be seen, which will be discussed further below. The initial coulombic efficiency of 79% indicates an irreversible capacity loss within the initial desodiation step. This is also typical for conversion reactions and a result of solid electrolyte interphase formation along with formation of a nanoscopic structure.[10b] The coulombic efficiency values were determined using $\eta_C = \frac{Q_{out}}{Q_{in}} \times 100\%$. As can be seen in **Figure 5**, the capacity further drops in the subsequent cycle by more than 200 mAh g^{-1}. This fading ends after around 25 cycles (≈400 mAh g^{-1}), after which the capacity increases again until the 150th cycle. The gradual activation of the electrode can be also seen from the derivative plots. Figure 4c shows that the peak positions shift during cycling for about 100 cycles after which the situation becomes stable (with a slight average increase of +0.35 mAh g^{-1} between the 100th and 200th cycle). Such a long-term activation over many cycles has been also reported by Park et al. for CuS by using the same electrolyte as in the present study.[18] It is important to note that carbon black also contributes to the storage capacity, see Figure S4 (Supporting Information). The maximum capacity of carbon black after the initial cycle is about 180 mAh g^{-1} in the applied voltage window. This means that the maximum contribution to the electrode is 54 mAh $g(Cu_3PS_4)^{-1}$, i.e., below 10% when considering stable cycling at capacities of around 600 mAh $g(Cu_3PS_4)^{-1}$. We therefore neglect the contribution of carbon black in the following discussion. The derivate plot accentuates voltage plateaus, i.e., the plateau at 1.42 V becomes clearly visible as a strong peak. This feature almost completely disappears upon cycling, being a first hint on some irreversible two-phase process taking place. It is unlikely that

© 2020 The Authors. Published by WILEY-VCH Verlag GmbH & Co. KGaA, Weinheim

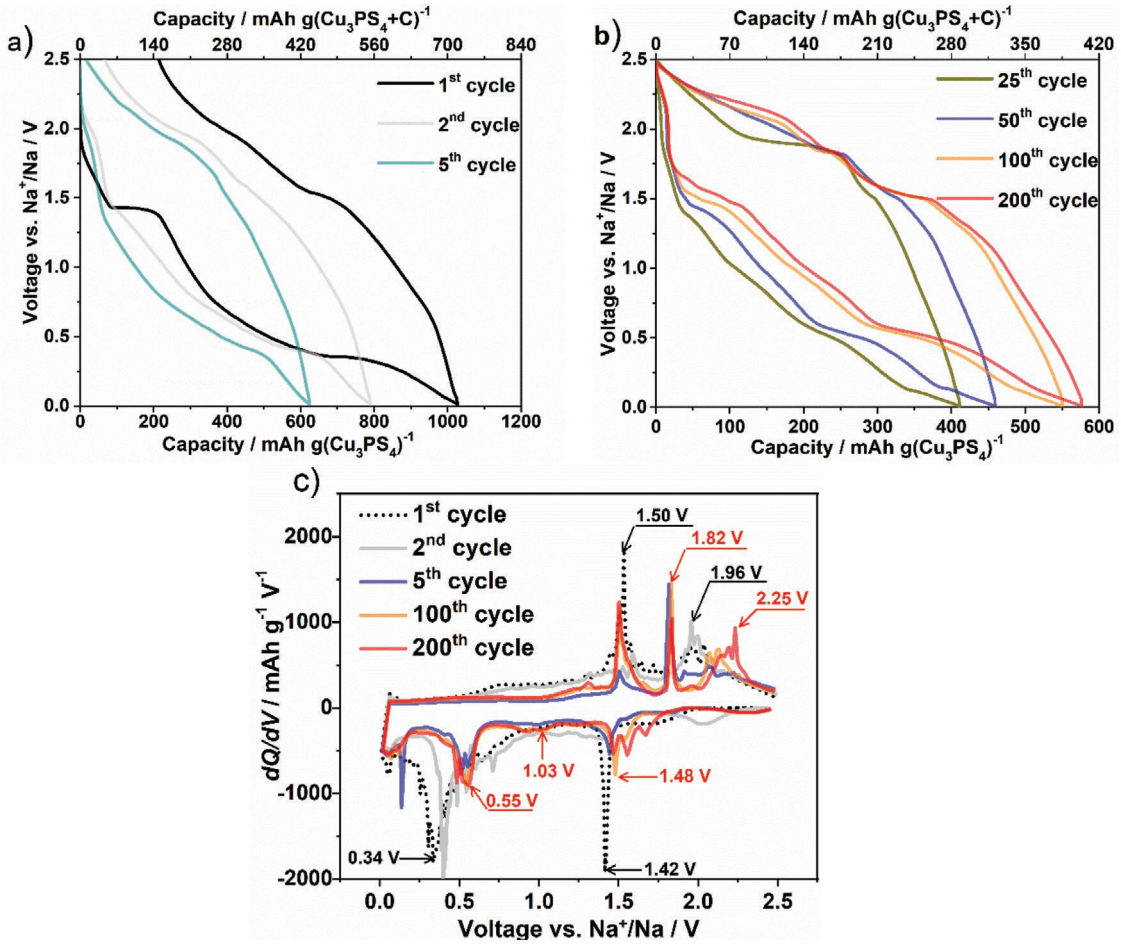

Figure 4. a) Voltage profiles of the 1st, 2nd, and 5th cycle. Cycling was performed with 1 M $NaPF_6$ in diglyme as electrolyte within a voltage window of 0.01–2.5 V versus Na^+/Na with a current density of 120 mA g^{-1}; b) voltage profiles of the 25th, 50th, 100th and 200th cycle; c) capacity derivative curves of the 1st, 2nd, 50th, 100th, and 200th cycle.

this feature relates to electrolyte decomposition as glymes are usually very stable at low potentials versus Na^+/Na. In the subsequent cycles, enhanced activity is found around 2 V. The intensity of the peaks increases upon cycling, indicating that the redox behavior changes. This is in line with the activation of the electrode seen from the galvanostatic measurements.

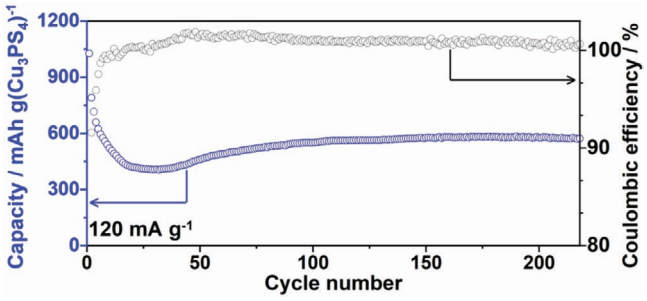

Figure 5. Discharge capacities versus cycle number and the corresponding Coulombic efficiencies for more than 200 cycles. Cycling was performed with 1 M $NaPF_6$ in diglyme as electrolyte within a voltage window of 0.01–2.5 V versus Na^+/Na with a current density of 120 mA g^{-1}.

Without further analysis, a redox activity around 2 V could be due to reduction/oxidation of sulfur and/or polysulfides.[28] The voltage profiles and corresponding derivate plots over 200 cycles show that, although the overall behavior is quite sloping, several steps repeatedly appear, indicating a multistep reaction process. According to the derivative plot, redox plateaus during reduction occur at around 1.5, 1.0, and 0.5 V. Plateaus during oxidation (desodiation) become more distinct during cycling, especially at higher cycling numbers (1.50 and 1.82 V). The third desodiation plateau is developing after around 100 cycles and shifts to voltages of about 2.25 V after 200 cycles. The combined overpotentials vary between about 0.6 to 1.0 V, being similar to many other sulfides/phosphides.[10a,b,18,29] Interestingly, the kinetics improve over cycling as the voltage gap of the hysteresis decreases. This decrease is likely the reason for the gradual increase in electrode capacity, as one can observe in Figure 5. In order to prove the reproducibility of the cycle life test, in total five cells were assembled being successfully cycled at least for 50 times. All of them showed the mentioned activation process reaching capacity values of at least 450 mAh $g(Cu_3PS_4)^{-1}$ so far. The capacities obtained for Cu_3PS_4 are higher than for CuS electrodes and enable enhanced cycling life in comparison

© 2020 The Authors. Published by WILEY-VCH Verlag GmbH & Co. KGaA, Weinheim

to the well-known CuP_2 when not using complex synthesis methods in order to create composites.[12b,18,30]

We further used impedance spectroscopy to qualitatively follow changes of the electrode during cycling. Figure S5a,b (Supporting Information) shows impedance spectra over several cycles (desodiated state). The overall resistance increases during the early cycles, which is generally associated with an increase in the charge transfer resistance. After that, the total resistance decreases again reaching values of about 10–16 Ω. This observation is in line with the gradual activation of the electrode discussed above.

For comparison, the electrodes were also tested in lithium half cells and with different electrolyte compositions and voltage windows, see Figures S6 and S7 (Supporting Information). In a previous study, we found a very strong influence of the conductive salt on reactions in diglyme based electrolytes, with NaOTf and $NaPF_6$ being preferred for sodium and graphite electrodes.[31] Figure S6 (Supporting Information) shows that, for lithium, the best capacity retention was found for a voltage window between 1–2.5 V versus Li^+/Li, with a capacity of 170 mAh $g(Cu_3PS_4)^{-1}$ retained after 200 cycles at 50 mA g^{-1} using 1 M LiTFSI in diglyme. Figure S7 (Supporting Information) shows results for various electrolyte compositions at two different current densities (50 and 120 mA g^{-1}). It is important to mention that a one-to-one comparison between $NaPF_6$ and $LiPF_6$ in diglyme is not possible as $LiPF_6$ forms solid complexes with diglyme. A similar behavior is found for $LiClO_4$.[32] Moreover, a selected carbonate electrolyte was tested and showed to be not appropriate for the use in Li and Na half cells, concluded from Figure S8 (Supporting Information). Among the various compositions tested, stable cycling at high capacity as well as an activation of the electrode is only found for $NaPF_6$ when using diglyme as solvent. In case of other salts as well as for the lithium half cells, a much lower capacity and rapid fading was observed. While further explanations on this behavior are outside the scope of this manuscript, it is clear that the electrolyte composition is very important for cycling the Cu_3PS_4 electrodes. The differences in electrode performance for varying electrolyte compositions are usually linked to a different solid electrolyte interphase formation. Further optimization of the electrolyte composition may therefore even lead to better results. The improved behavior for diglyme compared to carbonates is well in line with reports on copper sulfides, which also suffer from rapid capacity for the latter solvents.[14b] Interestingly, the sodium cells show higher capacities compared to the lithium cells in the diglyme-based electrolyte. This is also found for conversion reactions with copper diimide (CuNCN)[33] though usually the opposite trend is found, i.e., experimentally determined capacities for conversion reactions with lithium are typically higher than for the analogue reaction with sodium.

2.3. Postmortem Analysis of Cu_3PS_4

The reaction mechanism was studied by X-ray photoelectron spectroscopy (XPS) and (operando) X-ray diffraction. For this, the best performing electrodes, i.e., the electrodes cycled in $NaPF_6$ (1 M) diglyme were chosen. Before discussing the results, one has to realize that the redox chemistry of thiophosphates is very complex. Considering Cu_3PS_4, the formal oxidation states are Cu(+I), P(+V), and S(–II). During oxidation/reduction, all three elements can be redox active, e.g., Cu(+I) can be reduced to Cu(0) or oxidized to Cu(II), S(–II) can be oxidized to polysulfides S_x^{2-} or S(0), P(+V) may be reduced to P(+IV), P(0) or P(–III) and so on. P_2S_5 may also reappear as compound during the reaction. Moreover, a variety of thiophosphate anions exists, that may form during cycling as well. A discussion on the chemistry of lithium thiophosphates can be found in a review by Ghidiu et al.[34]

As conversion reactions are typically very complex in nature, it is generally difficult to clarify the redox chemistry. Part of the problem is that the reactions are often incomplete and, in many cases, amorphous and intermediate phases are formed. This becomes even more challenging for Cu_3PS_4 as all elements can be redox active. Moreover, the formation of often thick SEIs additionally aggravates the analysis of the bulk electrode. Nevertheless, in the following we attempt to at least confirm or exclude some of the possible reaction products using a more surface (XPS with depth profiling) and a bulk (XRD) sensitive technique. It is known that thiophosphates used as solid electrolytes react when exceeding their electrochemical stability window (≥2 V vs Li^+/Li), leading to excess capacity.[23b] During oxidation, S(0) formation is likely as well as the formation of P_2S_5 or anions like $P_2S_6^{2-}$, $P_2S_7^{4-}$, and $P_2S_8^{4-}$.[23a,c] Further side reactions with these decomposition products can occur during reduction at lower voltages of about 1.5 V, this way forming products like $Li_4P_2S_6$ as well as Li_3P and Li_2S.[23]

For the XPS studies, the pristine electrodes and the cycled electrodes after stabilization (50th cycle sodiated and desodiated state) were compared, see **Figure 6**. Ar^+-sputtering was applied to remove possible surface layers/SEI components (see the Characterization Methods for details). Figure 6a,b shows the high resolution S 2p and P 2p spectra for the pristine electrode. Results on Li_3PS_4 and Ag_3PS_4 served as reference for interpreting the data.[35] The spectra were in good agreement, which is reasonable considering that γ–Li_3PS_4, Ag_3PS_4 and Cu_3PS_4 share the same crystal structure and space group (*Pmn*21). Doublet peaks (energy separation = 1.2 eV) at binding energies (BE) of 162.0 eV for the S2p signal can be related to the transition metal-PS_4^{3-} bondings by comparison with literature data on Li_3PS_4 and Ag_3PS_4. A signal for PS_4^{3-} has been reported at 161.5 eV for Li_3PS_4,[35a] at 163.7 eV for crystalline Ag_3PS_4 and at 162.1 eV for amorphous Ag_3PS_4.[35b] The small deviations between the different thiophosphates are due to the different cations. Another peak at a BE of 163.5 eV was detected, corresponding to sulfur or other P–S compounds.[23c] Qiao et al. explain that amorphization leads to a shift of the P–S–P binding energies to lower values.[35b] Consequently, the overall broad peak related to the S2p signal may be also due to an overlay of crystalline and amorphous Cu_3PS_4. Note that there was no indication for other phases by XRD (Figure 1). Results for the cycled electrode are shown in Figure 6c–f. Figure 6c shows the S 2p spectrum of the electrode after sodiation. The peaks according to the S $2p_{3/2}$ and S $2p_{1/2}$ signals at 161.6 and 162.8 eV can be assigned to Na_2S,[36] which is an expected discharge end product according to Equation (2). This means that the tetrahedral coordinated P—S bonds cleave during sodiation.

© 2020 The Authors. Published by WILEY-VCH Verlag GmbH & Co. KGaA, Weinheim

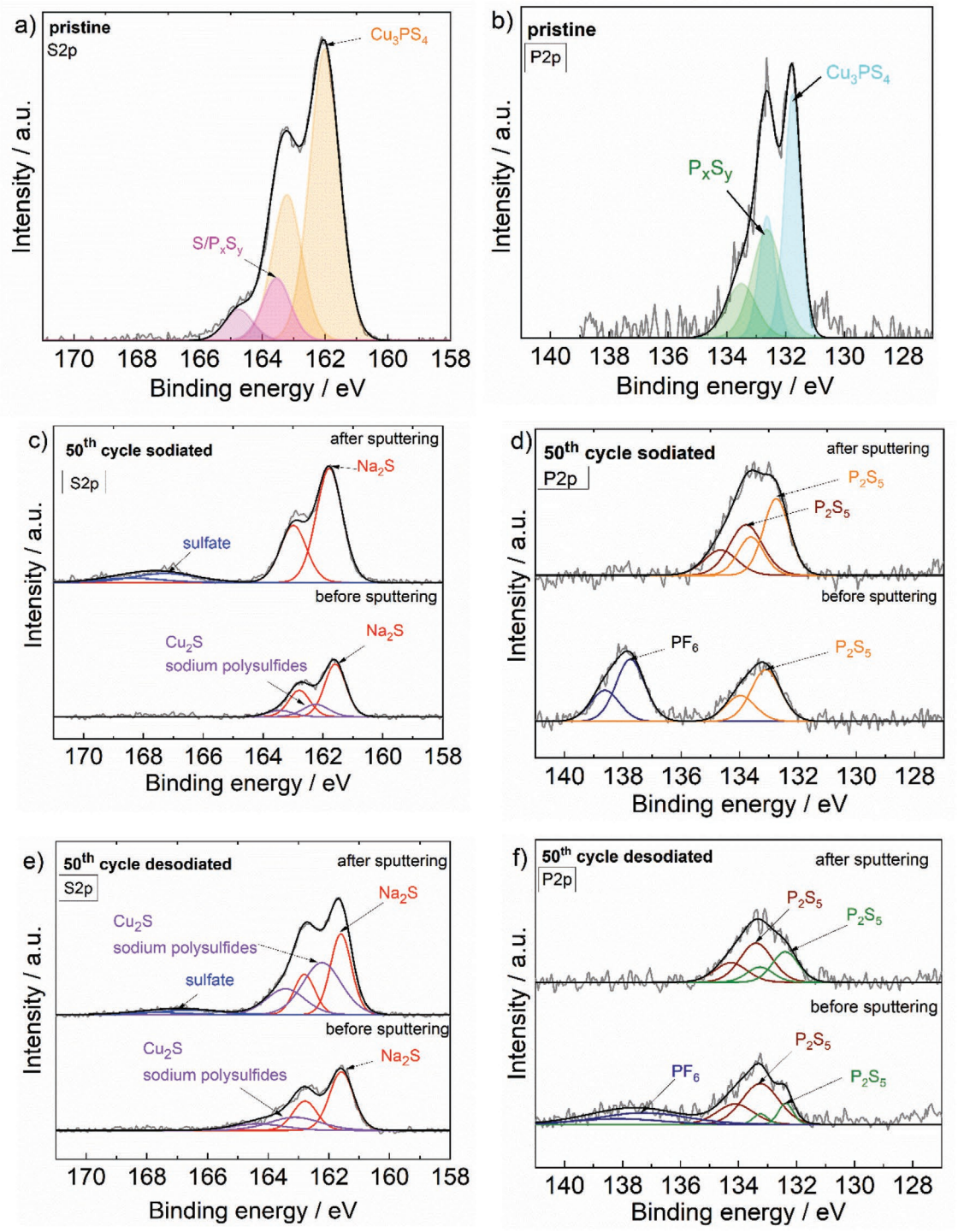

Figure 6. XPS analysis of the S 2p signal for a) pristine Cu_3PS_4; c) the sodiated state of the 50th cycle; e) the desodiated state of the 50th cycle. b,d,f) The corresponding P 2p signals are shown. The sputtering time was 30 min. Cycling was performed at 120 mA g^{-1} in a voltage window of 0.01–2.5 V versus Na^+/Na using 1 M $NaPF_6$ in diglyme as electrolyte.

Similarly, the P 2p signal has changed after sodiation, as can be seen in Figure 6d. The vanishing of the species marked in light blue at 131.8 eV ($P2p_{3/2}$) and 132.6 eV ($P2p_{1/2}$), indicates the P—S bond cleavage. This finding is in line with the results by Fan et al. and Edison et al. obtained for $FePS_3$ and $SnPS_3$.[25,26]

Figure 6e shows the S 2p spectrum after subsequent charging (50th cycle, desodiated state). Again, the signature of Na_2S can be found. However, the signal is broader, especially after removing the oxidic surface layer by sputtering with Ar^+-ions. This is an indication that residues of Na_2S remain inactive.[37]

© 2020 The Authors. Published by WILEY-VCH Verlag GmbH & Co. KGaA, Weinheim

Moreover, more sodium polysulfide compounds might be formed. The occurrence of other charging products such as Cu_3PS_4 or Cu_2S could not be clearly evidenced as the signals from Na polysulfides (161.7 eV/163.3 eV for terminal and central sulfur), PS_4^{3-} (162.1 eV) and Cu_2S (162.6 eV) are overlapping each other.[36,37]

Overall, the S 2p spectrum provides at least proof for the formation and (partial) decomposition of Na_2S during discharging/charging. The XPS data could not be used to confirm formation of elemental copper since the signals of Cu (I) (932.4 eV) and elemental Cu (932.6 eV) in the Cu $2p_{3/2}$ spectrum are extremely close.[38] Nevertheless, the data is shown in Figure S9a,b (Supporting Information). Little evidence for the presence of a small amount of Cu^{2+} (933.8 eV) can be found in the charged electrode, as it can be observed in Figure S9b (Supporting Information). This indicates that some CuO might be present in the sample. However, this contribution can be also due to a CuO impurity that formed during the short air exposure during sample transfer or formed by a side reaction with the diglyme electrolyte.

Figure 6b,d,f shows the results for the P 2p spectra. The pristine material shows a doublet at a BE of 131.8 eV due to PS_4^{3-} (again by comparison with Li_3PS_4).[23c,35a] Furthermore, another P—S bonding species can be seen at 132.6 eV, being either a sign for a local P_xS_y residue which might not have fully reacted to Cu_3PS_4 during synthesis or being due to the above mentioned existence of some amorphous Cu_3PS_4. As sulfur formally remains in the –II state during discharging, phosphorous may be redox active. As the oxidation state of P in Cu_3PS_4 is +V, reduction to lower oxidation states during sodiation is expected. However, formation of Cu_3P could be excluded, because no signal at BEs around 129–130 eV was detected.[39] There was also no evidence for elemental phosphorous, which should show signals at a BE of around 128 eV. The signal at around 133 eV fits to phosphates and thiophosphates, which may have formed due do side reactions or reactions with the electrolyte. The formation of Na_3P as the most likely discharge product (see Equation (2)) could not be confirmed. However, the corresponding binding energy at around 127 eV overlaps with signals of the Cu 3s spectrum at 126 eV, therefore complicating the analysis. Due to this overlap, no data <127 eV were acquired. Nevertheless, substantial formation of Na_3P during discharging can be excluded from the XPS data. After sodiation, P_2S_5 could be detected at 133.7 eV.[40] However, as formation of P_2S_5 cannot account for the large capacity values determined, it is expected to be only a minor component of the electrode. Consequently, the redox activity of phosphorus cannot be clearly clarified via XPS, but phosphorus could be evidenced as oxidized species with an oxidation state larger than zero in the sodiated and in the desodiated state as well. Dietrich et al. demonstrated that the occurrence of Li_2S in presence of P_2S_5 influences the P–S–P binding energy due to acting polarization forces.[40] Thus, we may observe an analogue case for Na, i.e., an overlay of shifted binding energies between 132–134 eV derived from P_2S_5 due to the presence of Na_2S is likely.

Before sputtering, the spectra of F 1s (687.7 eV) and P 2p (137.7 eV) show presence of PF_6^-, which remains from the conductive salt. The signals disappear by sputtering, indicating the conductive salt residues are located close to the electrode surface. Figure S9c,d (Supporting Information) shows evidence for NaF at a BE of 684.7 eV in the F 1s spectrum, which is an expected product of SEI formation.

The analysis by XPS leads to the following conclusions for the redox reactions after electrode activation (50th cycle): a) After sodiation as well as after desodiation, the presence of Cu_3P, Na_3P, P(0) and S(0) can be excluded; b) sodiation leads to formation of Na_2S, but not all of it disappears during desodiation; c) PS_4^{3-} could not be observed, meaning that Cu_3PS_4 is not an active compound during cycling, so it is irreversibly decomposed during electrode activation. However, very little P_2S_5 may be present; d) small amounts of Cu_2S in overlay with Na polysulfides may be present.

2.4. Operando XRD Analysis of Cu_3PS_4

Figure 7a shows operando XRD results for the 1st cycle. Upon sodiation, the Cu_3PS_4 reflections immediately start to disappear. This process is clearly linked to the voltage plateau at 1.4 V versus Na^+/Na. This plateau only appears during the first sodiation process, see also Figure 4a indicating that the structure of Cu_3PS_4 is irreversibly converted. At the same time, reflections due to Na_2S and Cu become more intense, which can be more clearly seen from the patterns after complete discharge and charge, looking at Figure 7b. The Na_2S signal intensity continuously increases with the degree of sodiation, reaching its maximum at the end of the discharge at 0.01 V versus Na^+/Na. This indicates that Na_2S continuously forms during sodiation. During subsequent desodiation (charging), the intensity of the reflections continuously decreases, yet complete disappearance does not take place. This indicates a partial reversibility of the Na_2S conversion during cycling, well in line with the XPS findings. Charge products could be polysulfides or elemental sulfur (the former being confirmed by XPS). Formation and disappearance of Na_2S could be also found in the 2nd cycle (cf. Figure 7b). Only minor changes in the intensity of the Cu (111) reflection are observed within the 2nd cycle, indicating a very small, if any, redox activity of copper during cycling, looking at Figures S10 and S11 (Supporting Information). The results therefore indicate that the high storage capacity of the electrode is due to sulfur redox. Also phosphorous might contribute, but neither XPS nor XRD could provide any evidence for this.

Considering this, the first cycle is clearly very different from all the others. As sulfur in Cu_3PS_4 is already in its fully reduced state, the initial sodiation capacity is largely linked to reduction of Cu^+ to Cu(0). Sulfur then becomes redox active during the first desodiaton step. In view of the very good cycle life for an electrode based on sulfur redox, one may therefore speculate that the formed copper nevertheless plays a role in improving the behavior of the electrode. This might be because the formed copper improves the local electronic conductivity and because copper can trap polysulfides (by forming, e.g., CuS and Cu_2S) that would otherwise dissolve into the electrolyte. Copper sulfides could also reversibly store charge in this electrolyte;[14b,18] however, XRD clearly shows that most of the copper remains in its metal state during cycling. The dominant role of the sulfur redox can also be rationalized from the experimentally determined capacity values which reach about

© 2020 The Authors. Published by WILEY-VCH Verlag GmbH & Co. KGaA, Weinheim

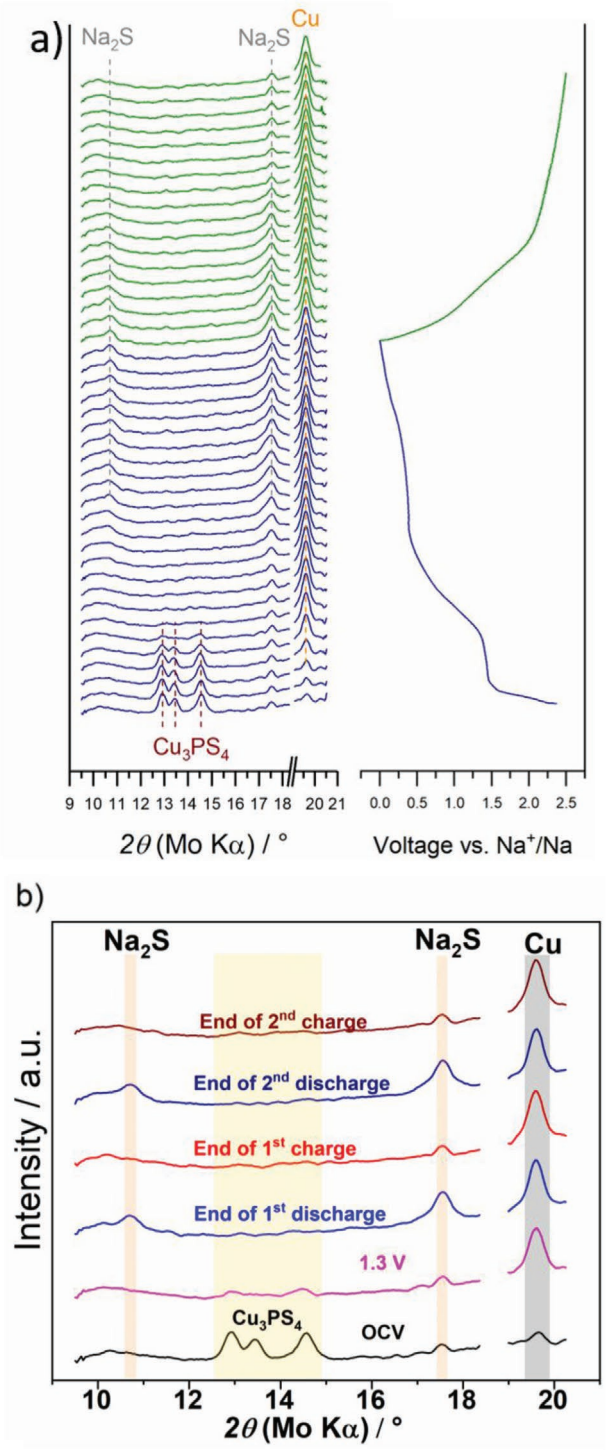

Figure 7. Operando XRD analysis after a) the initial sodiation and desodiation step. The crystalline nature of Cu_3PS_4 vanishes and Cu as well as Na_2S signals increase during sodiation. The measurement was performed continuously during recording the diffraction patterns. b) XRD patterns after completed sodiation and desodiation of the initial 2 cycles. Following references were used: Cu_3PS_4: ICSD: 98-041-2240 with the (210), (002) and (211) plane; Na_2S: ICSD: 98-006-0436 with the (111) and (022) plane and Cu: ICSD: 98-005-3755 with the (111) plane. Cycling was performed at 120 mA g^{-1} in a voltage window of 0.01–2.5 V versus Na^+/Na using 1 M $NaPF_6$ in diglyme as electrolyte.

580 mAh g^{-1} after more than 200 cycles. Assuming solely sulfur redox between S^{2-} and S^0, the capacity of the electrode (with the formal composition of Cu_3PS_4) would be 613 mAh $g(Cu_3PS_4)^{-1}$, i.e., the values are close to each other.

Finally, it is also worth noting that the long cycle life shown in Figure 5 implies that dissolution of the electrode components does not take place. This is not necessarily expected, as for example Na_2S in combination with P_2S_5 shows a high solubility in diglyme (the individual compounds do not).[41] Dissolution of the active material would lead to a rapid capacity fading. As XPS and XRD both provide evidence for Na_2S formation, the long cycle life directly implies that P_2S_5 does not occur in larger amounts during cycling.

2.5. Rate Performance and High Current Stability

Rate capability measurements are shown in **Figure 8**a. Even at current densities as high as 5 A g^{-1}, values around 350 mAh g^{-1} were obtained. After decreasing the current density again to 120 mA g^{-1}, the capacity recovered to values of about 600 mAh g^{-1}. The voltage profiles at different current densities are shown in Figure S12 (Supporting Information). Figure 8b shows the cycling stability test at a current rate of 1 A g^{-1}. The storage capacity exceeded more than 400 mAh g^{-1} even after 1400 cycles, indicating that the redox processes (after stabilization of the electrode) are highly reversible. Coulombic efficiency values obtained were ≈100% over the whole study. Selected voltage profiles and derivative plots are compared in Figure 8c,d and show that the redox behavior remains nearly constant over the long term test. Overall, compared to $FePS_3$,[25] Cu_3PS_4 performs better with respect to rate capability, cycling stability as well as capacity when cycled toward sodium.

3. Conclusion

The use of copper thiophosphate (Cu_3PS_4) as electrode for sodium-ion batteries was explored. Cu_3PS_4 was synthesized by reactive ball milling from Cu, sulfur and P_2S_5 and tested in half cells between 0.01 and 2.5 V versus Na^+/Na. Different electrolytes were tested with $NaPF_6$ (1 M) in diglyme, showing the best behavior. At 1 A g^{-1}, capacity values of around 450 mAh g^{-1} were obtained for more than 1400 cycles, indicating excellent reversibility of the reaction. The redox behavior was analyzed using (operando) XRD and XPS with depth profiling. During initial sodiation, Cu_3PS_4 undergoes a conversion reaction including the formation of copper and Na_2S. The PS_4^{3-} tetrahedrons are cleaved. During cycling, the redox activity is dominated by sulfur redox likely between S^{2-} and polysulfides S_x^{2-}. Some Na_2S seems to remain inactive during cycling, however. Copper seems to contribute to a minor degree during charge storage as Cu metal is found in the charged and discharged state; however, the intensities of the XRD reflections slightly vary during cycling. The role of phosphorous remains unclear so far. NMR spectroscopy may provide further information on this in the future. Overall, the processes appear highly reversible.

© 2020 The Authors. Published by WILEY-VCH Verlag GmbH & Co. KGaA, Weinheim

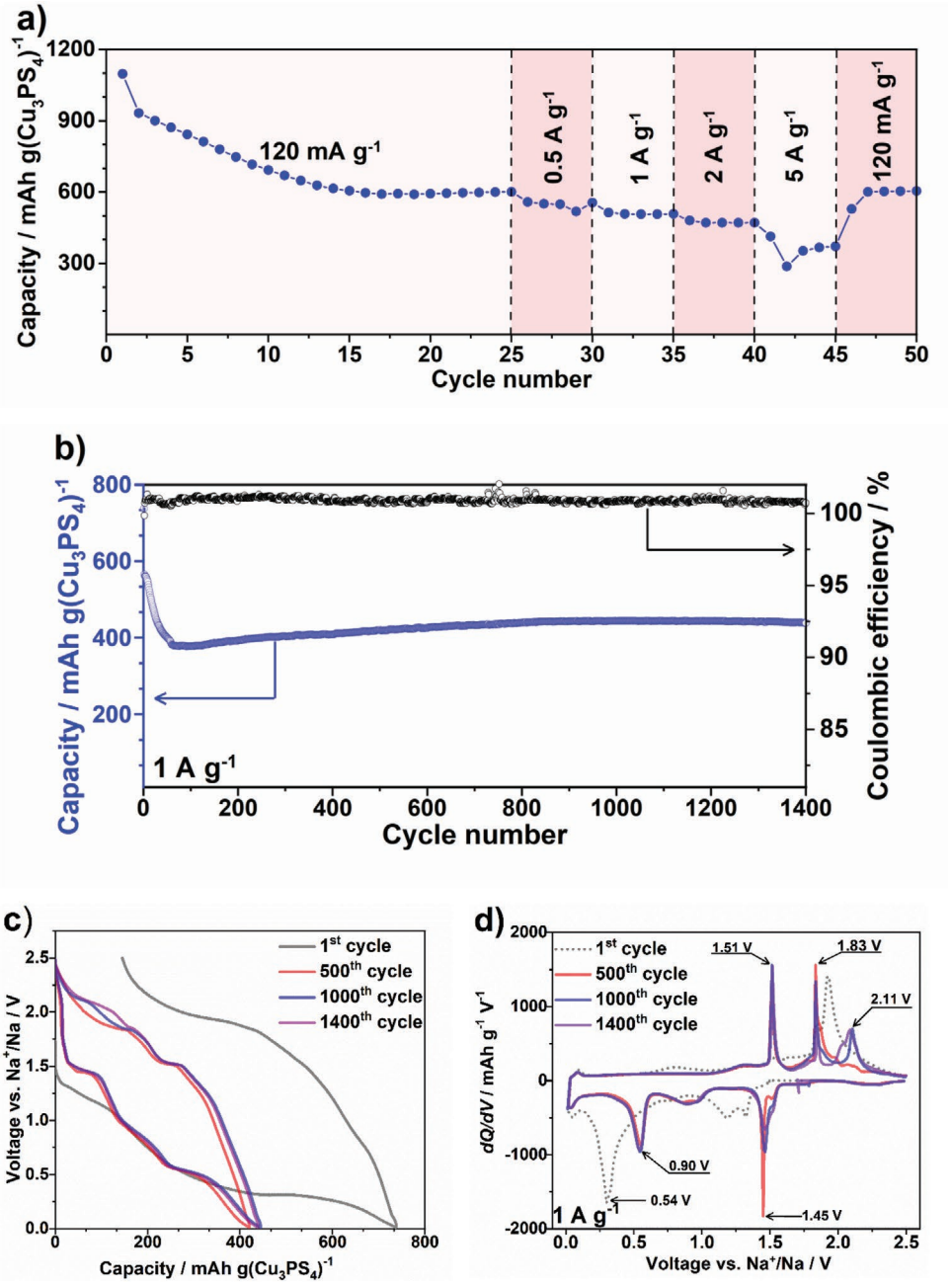

Figure 8. a) Rate capability for a Cu_3PS_4/C electrode with 1 M $NaPF_6$ in diglyme for a voltage window of 0.01–2.5 V; b) High current rate cycling performance test for a Cu_3PS_4/C electrode with 1 M $NaPF_6$ in diglyme for a voltage window of 0.01–2.5 V at 1 A g^{-1}; c) corresponding voltage profiles and d) capacity derivatives.

The remaining Cu metal may aid the electronic wiring of the electrode and act as a polysulfide trap, thereby improving cycle life. Reference experiments with the analogue lithium cell showed that the storage capacity of Cu_3PS_4 is higher for sodium. The lower voltage limit for achieving stable cycling is higher for Li (≈1 V vs Li^+/Li) compared to sodium (0.01 V vs Na^+/Na). Finally, we also demonstrated that the storage capacity of Cu_3PS_4 electrodes is higher compared to Cu_2S, CuS, Cu_3P, and $FePS_3$ and shows better cycling stability than Cu_3P, $FePS_3$ and CuP_2 electrodes.

4. Experimental Section

Preparation of the Electrodes: Commercial Cu particles (<425 µm, 99.5% purity), P_2S_5 (99% purity), and sulfur (99.5% purity) from Sigma Aldrich were used as active materials and were put in appropriate stoichiometric ratios into zirconia jars. 5 g of the raw materials were ball milled in a planetary ball mill (PBM, Fritsch Pulverisette 7) for 24 h at 400 rpm with a jar volume of 80 mL as well as in a subsequent step in a swing ball mill (SBM, Retsch MM 400) for 12 h with a jar volume of 10 mL applying a frequency of 25 Hz, this way forming a composite with carbon. Cu_3PS_4 to carbon weight ratio was set to 7:3. For the use of both ball mills, the ball to powder weight ratio was set to 10:1.

© 2020 The Authors. Published by WILEY-VCH Verlag GmbH & Co. KGaA, Weinheim

Electrode Preparation: A slurry, using 5 wt% of PVDF binder related to the total weight of Cu_3PS_4 powder was prepared in an NMP solution in an MBraun Glovebox under Ar atmosphere. The slurry was casted with a doctor blade by hand onto a copper foil (Schlenk) under inert conditions and the electrodes were cut into spherical 12 mm diameter pieces and dried in a vacuum tube oven at 70 °C overnight. The finally obtained active mass loadings varied between 1.5–2.2 mg cm^{-2}.

Characterization Methods: XRD analysis of the Cu_3PS_4 electrodes and powders was performed with a Bruker Phaser D2 diffractometer using Cu Kα radiation (0.02° step width and 20 s step time). XPS of the Cu_3PS_4/C electrodes was performed using a multiprobe system (Scienta Omicron) with a monochromatic X-ray source (Al Kα) and an electron analyzer (Argus CU) with an 0.6 eV spectral energy resolution. The spectra were fitted using Voigt functions after background subtraction. In order to remove the thin surface layer, consisting of salt rests and oxidized species, the samples were sputtered in the same multiprobe system using Ar^+ ions (FOCUS FDG150, 1 kEV, 10 mA) for 30 min. This corresponds to an approximate sputter depth of 15 nm. Longer sputter times did not change the spectra. TEM specimens were prepared by dispersing the powder in ethanol in an ultrasonic bath and placing onto a holey carbon copper grid. The structural features of the Cu_3PS_4 nanoparticles were studied by high-resolution transmission electron microscopy (HRTEM) and selected area electron diffraction in a JEOL JEM 3010HT operating at 300 kV that is equipped with a LaB_6 filament and a 1k × 1k GATAN multi scan CCD-camera. TEM investigations for getting information about the particle size (Figure S3a,b, Supporting Information) were carried out on a Philips CM200 LaB_6 operated at an acceleration voltage of 200 kV.

The operando XRD measurement was performed on an STOE Stadi MP diffractometer equipped with a Dectris Mythen 1K linear silicon strip detector and Ge(111) double-crystal monochromator (Mo Kα1 radiation) in a Bragg–Brentano geometry on a sepcifically developed operando half cell.[42] One XRD pattern was recorded every hour and the operando cell was cycled at C/20 in order to obtain one XRD pattern every 0.3 sodium atoms reacted per formula unit.

Electrochemical tests: Electrolytes were prepared by dissolving $NaPF_6$ (1 M) from Alfa Aesar in diglyme (Sigma Aldrich). Diglyme was dried over a molecular sieve (4 Å, Sigma Aldrich) to ensure the water content to be lower than 20 ppm, confirmed by Karl-Fisher titration. Other electrolyte solutions were prepared in the same way. Electrochemical measurements were performed in C2032 coin cells, using 2 pieces of glass microfiber filters (Whatman, GF/A) as separator and Na metal (BASF SE) as counter electrode. The electrochemical experiments were performed with a Biologic MPG2 and a BCS galvanostat/potentiostat. Reproducibility of the results was assured by cycling in total more than 20 cells. Impedance tests were carried out in beaker cells (two electrode system) and measured using a Biologic SP150 galvanostat/potentiostat.

Supporting Information

Supporting Information is available from the Wiley Online Library or from the author.

Acknowledgements

P.A., W.B., A.L.S., and J.R.B. acknowledge support from the German Research Foundation (DFG, 257682551), the Federal Ministry of Education and Research (BMBF, 03XP0026I) and the ESF fund (HyNIB, FGR 0055). Z.Z. is grateful for support from the CSC scholarship council. The authors thank Ms. Fähndrich for providing technical and experimental support. BASF SE is acknowledged for kindly providing high-purity sodium. AT and CN acknowledge support from the DFG Research Infrastructure Grant (INST 275/257-1 FUGG) and funding through ESF Research Group FGR 0092 "LiNaKon." M.R. and M.S. thank the German Research Foundation for financial support (RE 1261/19-1).

Conflict of Interest

The authors declare no conflict of interest.

Keywords

Cu_3PS_4, diglyme, Li-ion batteries, Na-ion batteries, reactive ball milling, thiophosphates

Received: December 20, 2019
Revised: February 14, 2020
Published online: March 13, 2020

[1] a) P. K. Nayak, L. Yang, W. Brehm, P. Adelhelm, *Angew. Chem., Int. Ed.* **2018**, *57*, 102; b) S.-W. Kim, D.-H. Seo, X. Ma, G. Ceder, K. Kang, *Adv. Energy Mater.* **2012**, *2*, 710; c) D. Kundu, E. Talaie, V. Duffort, L. F. Nazar, *Angew. Chem., Int. Ed.* **2015**, *54*, 3431; d) M. D. Slater, D. Kim, E. Lee, C. S. Johnson, *Adv. Funct. Mater.* **2013**, *23*, 947; e) N. Yabuuchi, K. Kubota, M. Dahbi, S. Komaba, *Chem. Rev.* **2014**, *114*, 11636; f) H. Pan, Y.-S. Hu, L. Chen, *Energy Environ. Sci.* **2013**, *6*, 2338; g) M. H. Han, E. Gonzalo, G. Singh, T. Rojo, *Energy Environ. Sci.* **2015**, *8*, 81.

[2] a) M. Li, Z. Du, M. A. Khaleel, I. Belharouak, *Energy Storage Mater.* **2020**, *25*, 520; b) H. Zhang, Y. Huang, H. Ming, G. Cao, W. Zhang, J. Ming, R. Chen, *J. Mater. Chem. A* **2020**, *8*, 1604.

[3] a) K. Kubota, S. Kumakura, Y. Yoda, K. Kuroki, S. Komaba, *Adv. Energy Mater.* **2018**, *8*, 1703415; b) B. Senthilkumar, C. Murugesan, L. Sharma, S. Lochab, P. Barpanda, *Small Methods* **2018**, *3*, 1800253; c) J. Qian, C. Wu, Y. Cao, Z. Ma, Y. Huang, X. Ai, H. Yang, *Adv. Energy Mater.* **2018**, *8*, 1702619.

[4] a) G. Piana, M. Ricciardi, F. Bella, R. Cucciniello, A. Proto, C. Gerbaldi, *Chem. Eng. J.* **2020**, *382*, 122934; b) J. Zhang, D.-W. Wang, W. Lv, L. Qin, S. Niu, S. Zhang, T. Cao, F. Kang, Q.-H. Yang, *Adv. Energy Mater.* **2018**, *8*, 1801361; c) J. Yang, H. Zhang, Q. Zhou, H. Qu, T. Dong, M. Zhang, B. Tang, J. Zhang, G. Cui, *ACS Appl. Mater. Interfaces* **2019**, *11*, 17109; d) F. Bella, F. Colo, J. R. Nair, C. Gerbaldi, *ChemSusChem* **2015**, *8*, 3668; e) J.-J. Kim, K. Yoon, I. Park, K. Kang, *Small Methods* **2017**, *1*, 1700219.

[5] a) Y. Li, Y. Lu, P. Adelhelm, M. M. Titirici, Y. S. Hu, *Chem. Soc. Rev.* **2019**, *48*, 4655; b) B. Jache, P. Adelhelm, *Angew. Chem., Int. Ed.* **2014**, *53*, 10169.

[6] M. Goktas, C. Bolli, E. J. Berg, P. Novák, K. Pollok, F. Langenhorst, M. v. Roeder, O. Lenchuk, D. Mollenhauer, P. Adelhelm, *Adv. Energy Mater.* **2018**, *8*, 1702724.

[7] a) W. Luo, F. Shen, C. Bommier, H. Zhu, X. Ji, L. Hu, *Acc. Chem. Res.* **2016**, *49*, 231; b) X. Dou, I. Hasa, D. Saurel, C. Vaalma, L. Wu, D. Buchholz, D. Bresser, S. Komaba, S. Passerini, *Mater. Today* **2019**, *23*, 87; c) C. Bommier, X. Ji, *Isr. J. Chem.* **2015**, *55*, 486.

[8] a) P. Senguttuvan, G. Rousse, V. Seznec, J.-M. Tarascon, M. R. Palacín, *Chem. Mater.* **2011**, *23*, 4109; b) L. Wu, D. Buchholz, D. Bresser, L. Gomes Chagas, S. Passerini, *J. Power Sources* **2014**, *251*, 379; c) S. K. Das, B. Jache, H. Lahon, C. L. Bender, J. Janek, P. Adelhelm, *Chem. Commun.* **2016**, *52*, 1428; d) X. Ma, K. An, J. Bai, H. Chen, *Sci. Rep.* **2017**, *7*, 162; e) F. Bella, A. B. Munoz-Garcia, F. Colo, G. Meligrana, A. Lamberti, M. Destro, M. Pavone, C. Gerbaldi, *ACS Omega* **2018**, *3*, 8440.

[9] a) W. Brehm, J. R. Buchheim, P. Adelhelm, *Energy Technol.* **2019**, *7*, 1900389; b) T. Palaniselvam, M. Goktas, B. Anothumakkool, Y. N. Sun, R. Schmuch, L. Zhao, B. H. Han, M. Winter, P. Adelhelm, *Adv. Funct. Mater.* **2019**, *29*, 1900790; c) L. Xiao, Y. Cao, J. Xiao, W. Wang, L. Kovarik, Z. Nie, J. Liu, *Chem. Commun.* **2012**, *48*, 3321; d) A. Darwiche, R. Dugas, B. Fraisse, L. Monconduit, *J. Power*

© 2020 The Authors. Published by WILEY-VCH Verlag GmbH & Co. KGaA, Weinheim

Sources **2016**, *304*, 1; e) V. L. Chevrier, G. Ceder, *J. Electrochem. Soc.* **2011**, *158*, A1011; f) H. Xie, X. Tan, E. J. Luber, B. C. Olsen, W. P. Kalisvaart, K. L. Jungjohann, D. Mitlin, J. M. Buriak, *ACS Energy Lett.* **2018**, *3*, 1670.

[10] a) F. Klein, B. Jache, A. Bhide, P. Adelhelm, *Phys. Chem. Chem. Phys.* **2013**, *15*, 15876; b) J. Cabana, L. Monconduit, D. Larcher, M. R. Palacin, *Adv. Mater.* **2010**, *22*, E170; c) K. Cao, T. Jin, L. Yang, L. Jiao, *Mater. Chem. Front.* **2017**, *1*, 2213.

[11] F. Klein, R. Pinedo, P. Hering, A. Polity, J. Janek, P. Adelhelm, *J. Phys. Chem. C* **2016**, *120*, 1400.

[12] a) C. Kim, H. Kim, Y. Choi, H. A. Lee, Y. S. Jung, J. Park, *ACS Omega* **2018**, *3*, 7655; b) F. Zhao, N. Han, W. Huang, J. Li, H. Ye, F. Chen, Y. Li, *J. Mater. Chem. A* **2015**, *3*, 21754; c) S. Liu, X. He, J. Zhu, L. Xu, J. Tong, *Sci. Rep.* **2016**, *6*, 35189; d) J. Zhu, Q. He, Y. Liu, J. Key, S. Nie, M. Wu, P. K. Shen, *J. Mater. Chem. A* **2019**, *7*, 16999; e) E. J. Sheets, W.-C. Yang, R. B. Balow, Y. Wang, B. C. Walker, E. A. Stach, R. Agrawal, *J. Mater. Res.* **2015**, *30*, 3710.

[13] M. C. Stan, R. Klöpsch, A. Bhaskar, J. Li, S. Passerini, M. Winter, *Adv. Energy Mater.* **2013**, *3*, 231.

[14] a) Z. Hu, Q. Liu, S. L. Chou, S. X. Dou, *Adv. Mater.* **2017**, *29*, 1700606; b) B. Jache, B. Mogwitz, F. Klein, P. Adelhelm, *J. Power Sources* **2014**, *247*, 703.

[15] Y. Han, Y. Wang, W. Gao, Y. Wang, L. Jiao, H. Yuan, S. Liu, *Powder Technol.* **2011**, *212*, 64.

[16] A. Débart, L. Dupont, R. Patrice, J. M. Tarascon, *Solid State Sci.* **2006**, *8*, 640.

[17] Y. Wang, X. Zhang, P. Chen, H. Liao, S. Cheng, *Electrochim. Acta* **2012**, *80*, 264.

[18] J. Y. Park, S. J. Kim, J. H. Chang, H. K. Seo, J. Y. Lee, J. M. Yuk, *Nat. Commun.* **2018**, *9*, 922.

[19] Deutsche Rohstoffagentur, Preistrendmonitor, https://www.deutsche-rohstoffagentur.de/DE/Themen/Min_rohstoffe/Produkte/Preistrendmonitor/Preistrendmonitor-2019_06.pdf?__blob=publicationFile&v=4 (accessed: February 2020).

[20] Bildungsministerium fuer Bildung und Forschung, Phosphor-recycling–Abwasser und Klärschlamm als Quelle eines wertvollen Stoffs, http://ressourcewasser.fona.de/reports/bmbf/annual/2010/nb/German/401050/-2_1_05-phosphorrecycling-abwasser-und-klaerschlamm-als-quelle-eines-wertvollen-stoffs.html (accessed: February 2020).

[21] E. Sesay, TFI '19: Sulphur sentiment dampened by weak downstream demand, high stocks, https://www.icis.com/explore/resources/news/2019/09/20/10420493/tfi-19-sulphur-sentiment-dampened-by-weak-downstream-demand-high-stocks (accessed: February 2020).

[22] a) K. Xu, *Chem. Rev.* **2014**, *114*, 11503; b) T. Famprikis, P. Canepa, J. A. Dawson, M. S. Islam, C. Masquelier, *Nat. Mater.* **2019**, *18*, 1278; c) Z. Liu, W. Fu, E. A. Payzant, X. Yu, Z. Wu, N. J. Dudney, J. Kiggans, K. Hong, A. J. Rondinone, C. Liang, *J. Am. Chem. Soc.* **2013**, *135*, 975; d) Z. Ma, H.-G. Xue, S.-P. Guo, *J. Mater. Sci.* **2018**, *53*, 3927; e) Ö. U. Kudu, T. Famprikis, B. Fleutot, M.-D. Braida, T. Le Mercier, M. S. Islam, C. Masquelier, *J. Power Sources* **2018**, *407*, 31; f) T. Famprikis, J. A. Dawson, F. Fauth, O. Clemens, E. Suard, B. Fleutot, M. Courty, J.-N. Chotard, M. S. Islam, C. Masquelier, *ACS Mater. Lett.* **2019**, *1*, 641; g) A. L. Santhosha, P. K. Nayak, K. Pollok, F. Langenhorst, P. Adelhelm, *J. Phys. Chem. C* **2019**, *123*, 12126.

[23] a) R. Koerver, F. Walther, I. Aygün, J. Sann, C. Dietrich, W. G. Zeier, J. Janek, *J. Mater. Chem. A* **2017**, *5*, 22750; b) G. F. Dewald, S. Ohno, M. A. Kraft, R. Koerver, P. Till, N. M. Vargas-Barbosa, J. Janek, W. G. Zeier, *Chem. Mater.* **2019**, *31*, 8328; c) D. H. S. Tan, E. A. Wu, H. Nguyen, Z. Chen, M. A. T. Marple, J.-M. Doux, X. Wang, H. Yang, A. Banerjee, Y. S. Meng, *ACS Energy Lett.* **2019**, *4*, 2418; d) T. Hakari, M. Nagao, A. Hayashi, M. Tatsumisago, *J. Power Sources* **2015**, *293*, 721; e) N. Tanibata, M. Deguchi, A. Hayashi, M. Tatsumisago, *Chem. Mater* **2017**, *29*, 5232.

[24] a) F. Han, Y. Zhu, X. He, Y. Mo, C. Wang, *Adv. Energy Mater.* **2016**, *6*, 1501590; b) B. V. Lotsch, J. Maier, *J. Electroceram.* **2017**, *38*, 128; c) Y. Zhu, X. He, Y. Mo, *ACS Appl. Mater. Interfaces* **2015**, *7*, 23685; d) Y. Zhu, X. He, Y. Mo, *J. Mater. Chem. A* **2016**, *4*, 3253.

[25] C.-Y. Fan, X.-H. Zhang, Y.-H. Shi, H.-Y. Xu, J.-P. Zhang, X.-L. Wu, *J. Mater. Chem. A* **2019**, *7*, 1529.

[26] E. Edison, A. Chaturvedi, H. Ren, S. Sreejith, C. T. Lim, S. Madhavi, *ACS Appl. Energy Mater.* **2018**, *1*, 5772.

[27] X. Yin, S. A. McClary, Z. Song, D. Zhao, B. Graeser, C. Wang, N. Shrestha, X. Wang, C. Chen, C. Li, K. K. Subedi, R. J. Ellingson, W. Tang, R. Agrawal, Y. Yan, *J. Mater. Chem. A* **2019**, *7*, 4604.

[28] L. Medenbach, P. Adelhelm, *Top. Curr. Chem.* **2017**, *375*, 81.

[29] M. Fan, Y. Chen, Y. Xie, T. Yang, X. Shen, N. Xu, H. Yu, C. Yan, *Adv. Funct. Mater.* **2016**, *26*, 5019.

[30] a) J. Li, D. Yan, T. Lu, W. Qin, Y. Yao, L. Pan, *ACS Appl. Mater. Interfaces* **2017**, *9*, 2309; b) S. Kaushik, J. Hwang, K. Matsumoto, Y. Sato, R. Hagiwara, *ChemElectroChem* **2018**, *5*, 1340.

[31] M. Goktas, C. Bolli, J. Buchheim, E. J. Berg, P. Novak, F. Bonilla, T. Rojo, S. Komaba, K. Kubota, P. Adelhelm, *ACS Appl. Mater. Interfaces* **2019**, *11*, 32844.

[32] J. Grondin, *Solid State Ionics* **2004**, *166*, 441.

[33] A. Eguia-Barrio, E. Castillo-Martínez, F. Klein, R. Pinedo, L. Lezama, J. Janek, P. Adelhelm, T. Rojo, *J. Power Sources* **2017**, *367*, 130.

[34] M. Ghidiu, J. Ruhl, S. P. Culver, W. G. Zeier, *J. Mater. Chem. A* **2019**, *7*, 17735.

[35] a) A. Kato, H. Kowada, M. Deguchi, C. Hotehama, A. Hayashi, M. Tatsumisago, *Solid State Ionics* **2018**, *322*, 1; b) A. Qiao, H. Tao, Y. Yue, *J. Non-Cryst. Solids* **2019**, *521*, 119476.

[36] C.-H. Kuo, Y.-T. Chu, Y.-F. Song, M. H. Huang, *Adv. Funct. Mater.* **2011**, *21*, 792.

[37] M. Fantauzzi, B. Elsener, D. Atzei, A. Rigoldi, A. Rossi, *RSC Adv.* **2015**, *5*, 75953.

[38] A. V. Naumkin, A. Kraut-Vass, S. W. Gaarenstroom, C. J. Powel, NIST Standard Reference Database 20, Version 4.1, https://doi.org/10.18434/T4T88K (accessed: December 2019).

[39] Y.-C. Chen, Z.-B. Chen, Y.-G. Lin, Y.-K. Hsu, *ACS Sustainable Chem. Eng.* **2017**, *5*, 3863.

[40] C. Dietrich, R. Koerver, M. W. Gaultois, G. Kieslich, G. Cibin, J. Janek, W. G. Zeier, *Phys. Chem. Chem. Phys.* **2018**, *20*, 20088.

[41] L. Medenbach, P. Hartmann, J. Janek, T. Stettner, A. Balducci, C. Dirksen, M. Schulz, M. Stelter, P. Adelhelm, *Energy Technol.* **2020**, https://onlinelibrary.wiley.com/doi/full/10.1002/ente.201901200.

[42] J.-C. Jumas, M. T. Sougrati, A. Perea, L. Aldon, J. Olivier-Fourcade, *Hyperfine Interact.* **2013**, *217*, 107.

© 2020 The Authors. Published by WILEY-VCH Verlag GmbH & Co. KGaA, Weinheim